



Active Air Injection Control to Enhance Performance of Hollow-bladed Axial Fan: A Numerical Study

A. Bouanik^{1,2,3†}, T. Azzam², N. Abbasnezhad³, A. Larabi², M. Mekadem² and F. Bakir³

¹ *Research Laboratory in Energetics, Flows and Transfers, Military Academy of Cherchell, Tipaza, 42067, Algeria*

² *Laboratory of Fluid Mechanics, Military Polytechnical school, Bordj El Bahri, 16046, Algiers, Algeria*

³ *Arts et Métiers Institute of Technology, CNAM, LIFSE, HESAM University, Paris, 75013, France*

†Corresponding Author Email: d.bouanik.ayoub@emp.mdn.dz

ABSTRACT

Nowadays, axial fans participate in the most important areas of industry and research, including aviation, navy, wind tunnels, cooling towers, and even automobiles. Thus, more emphasis has been placed on improving their aerodynamic performances. It is important to notice that the parameters involved in designing a fan are mainly concerned with aerodynamic power, torque and efficiency. This study investigates the utilization of flow control techniques to improve performances of an axial fan equipped with hollow blades, shroud, and hub. These features grant the fan crucial characteristics, namely, its lightweight and facilitate the blowing action by taking advantage on its hollow parts. The fan's performance is evaluated using a steady RANS numerical model with a $k-\omega$ SST turbulence closure, which was validated with experimental data. An active control air blowing through a slot was introduced with various positions and dimensions. The results demonstrate a significant improvement in the fan's performance, with an up to 56% increase in aerodynamic power gain, accompanied by changes in the overall flow topology, noticed by closely analyzing the flow structure near the tip clearance.

Article History

Received August 2, 2023

Revised October 12, 2023

Accepted October 15, 2023

Available online January 1, 2024

Keywords:

Active control

Axial fan

Hollow blade

Hollow shroud ring

Leakage flow

Slot

1. INTRODUCTION

Axial fans are commonly used across various industrial applications to facilitate the movement of large air volumes. Nevertheless, their efficiency often encounters limitations stemming from challenges such as flow separation and the presence of boundary layers on the blade surfaces. These issues result in significant energy losses. One promising approach to address these concerns involves active air injection control, which entails introducing high-speed air into the boundary layer. This injection serves mainly to delay flow separation. However, it's worth noting that this technique may, under certain circumstances, negatively affect the fan's overall performance, generating issues related to torque, vibrations, and noise levels. Consequently, it becomes imperative to gain a comprehensive understanding of the underlying physics behind these phenomena to develop effective control strategies.

Among the various phenomena that can negatively affect performance, one of the most crucial is the occurrence of leakage flow within gap clearances under the effects of pressure difference close to the fan's tip,

which is the primary focus of this study. These clearance gaps are essential to accommodate any potential motor shaft vibrations or eccentricities when fans are enclosed within casings, particularly in sectors like automotive cooling. However, it's worth noting that this clearance gap can have a significant impact on the aerodynamic and acoustic performance of the fan, and it's crucial to recognize that improving these aspects constitutes the central aim of this study. In this regard, several researchers have investigated the influence of tip clearance gaps and leakage flow on the aerodynamic and acoustic performances of axial fans. Noteworthy contributions in this regard come numerically from (You et al., 2006; Boudet et al., 2015; Pogorelov et al., 2016; Luo et al., 2017; Heinrich et al., 2020; Hur et al., 2021). In addition to in-depth experimental studies such as (Kameier & Neise, 1997; Fischer et al., 2013; Zhu & Carolus, 2013; Canepa et al., 2016, 2019).

The findings of these studies have served as a source of inspiration for researchers, motivating them to explore both active and passive flow control strategies in turbomachinery. When it comes to passive control strategies, one potential approach involves geometrical

NOMENCLATURE			
λ	axial distance of rotating domain	Ψ	pressure coefficient $\Psi = \frac{2\Delta P}{(\rho u^2)}$
c	blade's chord length	ΔP	pressure difference generated by the fan
Φ	flow coefficient $\Phi = \frac{4Q_v}{(\pi D^2 u)}$	α	radial distance of rotating domain
Q_v	flow rate	RD	Rotating Domain
q_{inj}	injection flow rate	SST	Shear Stress Transport
ξ	injection rate	d	slot dimension
q_{max}	maximum flow rate	ω	specific dissipation rate
MRF	moving Reference Frame	T_1	tip clearance gap
N	node size	u	tip velocity
Y^+	non-dimensional wall distance	ϵ	turbulent dissipation rate
D	overall fan diameter	k	turbulent kinetic energy

modifications to the casing, as demonstrated by (Nadeau, 2005; Buisson et al., 2013; Park et al., 2019). Furthermore, passive control strategies also include modifications to the rotor, as examined by (Wallis et al., 2001; Chen et al., 2017; Heinrich et al., 2020). However, only a limited number of studies have investigated the use of active air injection control in axial fans. Which represents a promising approach with the capacity to augment the aeroacoustic efficiency of turbomachinery. This method achieves its potential by mitigating detrimental phenomena, particularly those associated with leakage flow, tip leakage vortex, and boundary layer separation, through the integration of supplementary energy. Numerous scholars, such as (Morris & Foss, 2001; Neuhaus & Neise, 2007; Sheng & Zhao, 2017; Chen et al., 2022), along with noteworthy references collected in the comprehensive review conducted by (Tiainen et al., 2018), have explored and documented this technique

In this investigation, we study a new generation of fan with hollow blades, Shroud and hub, known for their lightweight, high efficiency and low motor energy requirements to achieve the desired rotational speed. Several prior studies have examined this new generation of fans, with notable contributions from researchers such as (Sarraf et al., 2011; Azzam et al., 2017; Lucas et al., 2019; Pereira et al., 2021). Importantly, these works investigate the same type of hollow-bladed fan as the one under investigation in our current study. Furthermore, among these studies, (Azzam et al., 2017; Pereira et al., 2021) investigated the effectiveness of active flow control through air injection via holes in the periphery of the fan's rotating shroud ring to enhance its performance by reducing leakage flow in the gap clearance, both through experimental and numerical methods. It's also noteworthy that (Eberlinc et al., 2009) explored a different type of hollow-bladed fan, utilizing self-induced blowing to enhance its aerodynamic characteristics. He evaluated the influence of the interaction between two flows within the gap clearance zone on aerodynamic performance. The first flow represents the main flow generated by the fan itself, while the second flow originates from the fan's hollow blades.

In summary, this study aims to provide a comprehensive analysis of the effectiveness of active air injection through a slot along the entire periphery of the fan's shroud ring, originating from the hollow blades, with the objective of enhancing its performance. This analysis

takes into account varying factors such as rotation speed, injection rate, slot dimensions, and position to assess its influence on flow characteristics, topology, leakage flow, and torque. The control strategy employed in this study has resulted in significant improvements in aerodynamic performance by transforming the flow topology from axial to radial downstream of the fan. This transformation has the potential to expand the application of axial fans to confined spaces, including those affected by downstream blocking effects caused by system components installed near the fan exit.

2. CFD MODELLING AND SIMULATION

This section describes the methodology used for CFD modelling and simulation of an axial fan with hollow blades and a hollow rotating shroud ring (Fig. 1). The fan has six blades and a tip diameter of 358 mm, with detailed parameters available in (Sarraf et al., 2011). The fan is equipped with a rotating shroud to enhance mechanical strength, resulting in an overall tip diameter of approximately 390 mm. The hub has a diameter of 131 mm, and the blade chord length varies between 65 mm at the hub and 72 mm at the shroud. The hollow blades and shroud allow for secondary flow control towards the tip leakage or fan periphery, with the shroud being strong enough to support geometric modifications and the creation of slots for the active air injection control strategy adopted in subsequent analyses.

To ensure accuracy and build on previous research, a detailed numerical study of the complete calculation domain, which includes the actual fan geometry and test bench, was conducted. The study includes two fluid domains at the inlet and outlet and uses a separate rotating domain for each diaphragm diameter to improve results



Fig. 1 Fan with hollow blades and shroud ring (Azzam et al., 2017)

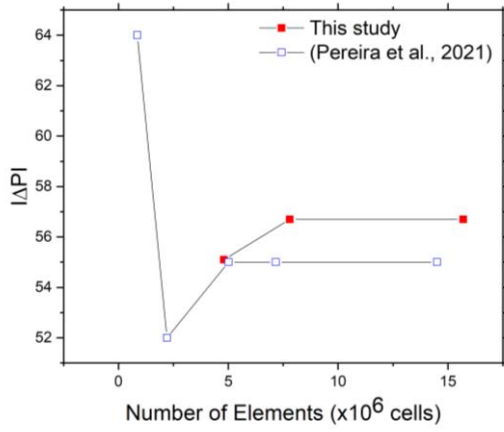


Fig. 2 Mesh sizes for grid dependency analysis

compared to experimental data. Control volumes mesh were used to capture important phenomena, such as tip clearance, fan blades, shroud, and hub zones, and predicted jet structures in the test bench through the diaphragm. Five diaphragm diameters are tested in this study 238, 267, 300, 336 and 375 mm. In order to evaluate the impact of grid density on the precision and convergence rate of the numerical solution, the mesh independency analysis was performed at the diaphragm diameter of 300 mm with rotation speed of 1500 rpm, by divided the mesh configuration around the fan, into two distinct zones as shown in (Fig. 4 c and d). The first zone is the boundary layer mesh (Fig. 4 d), situated in close proximity to the fan's wall. This mesh has been meticulously refined by adding an twelve (12) prism layers to the fan's walls, with the first layer measuring 0.04 mm in size. This refinement aims to achieve a maximum y^+ value of approximately 1, particularly on the fan walls, while the minimum value is approximately 0.2. These values ensure an appropriate level of detail in the near-wall region for accurate analysis. The second zone encompasses the area extending from the termination of the first zone to the region farther away from the fan (Fig. 4 c), which is the focus of our mesh study by investigating three distinct grid sizes (Fig. 2), obtained by varying the maximum node size of the control volume around the fan zone. The coarse grid (Grid-1) has a maximum node size of $N = 8$ mm, the fine mesh (Grid-2) has a value of $N = 3$ mm, and the refined grid (Grid-3) with $N = 2$ mm. More details of test bench design and the adopted mesh topology are depicted in (Fig. 2), (Fig. 3) and (Fig. 4) (Azzam et al., 2017; Pereira et al., 2021; International Organization for Standardization, 2007).

The simulations were conducted using ANSYS Fluent with finite volume discretization. The boundary conditions for the simulations are shown in (Fig. 3 b) and included atmospheric pressure at both the inlet and outlet, as well as non-slip conditions applied to the walls. To model fan rotation, a Moving Reference Frame approach was used with two specified rotational speeds (1000 and 2000 rpm) in the rotating domain. The momentum equations were solved using the MUSCL third-order scheme, while the other equations were solved using second-order schemes. Turbulence intensity was set to 1%, and the turbulent viscosity ratio was set to 1. In order to accurately predict largely separated flows, the K- ω SST

two-equations model was used and coupled with the Reynolds Averaged Navier-Stokes formulation. This model, is widely used in turbomachinery and complex flows with flow separation in the near-wall zone, particularly in the presence of an adverse pressure gradient, blends the k- ω model in the near-wall region with the k- ϵ model in the free-flow region, resulting in highly precise predictions of critical phenomena. These phenomena and model accuracy have been extensively examined in a variety of research studies, including those conducted by (Yadegari & Bak Khoshnevis, 2020a,b; Yadegari, 2021; Yadegari & Bak Khoshnevis, 2021; Haghighatjoo et al., 2022; Larabi et al., 2022)

In the context in Computational Fluid Dynamics (CFD) systems, it is of utmost importance to explicitly reference the governing equations that encapsulate the fundamental physical principles underlying the system, along with elucidating the methodologies employed for fo system closing to achieve convergence and solving this intricate system. The equations governing the three-dimensional steady-state, incompressible, viscous, turbulent flow as depicted in (Yadegari & Bak Khoshnevis, 2020b) consist of continuity Eq. (1) and momentum Eq. (2) equations, which can be expressed as follows:

$$\frac{\partial \bar{u}_i}{\partial x_i} = 0 \quad (1)$$

$$\rho \left[\bar{u}_j \frac{\partial \bar{u}_i}{\partial x_j} \right] = - \frac{\partial \bar{P}}{\partial x_i} + \frac{\partial}{\partial x_j} \left(\mu \frac{\partial \bar{u}_i}{\partial x_j} - \rho \overline{u'_i u'_j} \right) \quad (2)$$

In this context, \bar{u}_i and \bar{u}_j represent the mean velocity components, while μ denotes dynamic viscosity, P stands for pressure, and ρ signifies density. Furthermore, u'_i and u'_j represent the fluctuating velocity components. Additionally. The k- ω SST model combines two equations to describe the turbulent flow: one for turbulence kinetic energy (k) and another for specific rate of turbulence dissipation (ω).

$$\frac{\partial k}{\partial t} + u_j \frac{\partial k}{\partial x_j} = P_k - \beta^* k \omega + \frac{\partial}{\partial x_j} \left[(\vartheta + \sigma_k \vartheta_t) \frac{\partial k}{\partial x_j} \right] \quad (3)$$

$$\frac{\partial \omega}{\partial t} + u_j \frac{\partial \omega}{\partial x_j} = \alpha S^2 - \beta \omega^2 + \frac{\partial}{\partial x_j} \left[(\vartheta + \sigma_\omega \vartheta_t) \frac{\partial \omega}{\partial x_j} \right] + 2(1 - F_1) \sigma_{\omega 2} \frac{1}{\omega} \frac{\partial k}{\partial x_i} \frac{\partial \omega}{\partial x_i} \quad (4)$$

Equation Eq. (5) governs the determination of constants, transitioning from the region close to walls to the region distant from walls.

$$\varphi = \varphi_1 F_1 + \varphi_2 (1 - F_1) \quad (5)$$

Where F_1 is determined based on Eq. (6), which is provided below. The value of F_1 undergoes a transition from 1 in the vicinity of the wall to 0 as the distance from the wall increases.

$$F_1 = \tanh \left\{ \left\{ \min \left[\max \left(\frac{\sqrt{k}}{\beta^* \omega y}, \frac{500 \vartheta}{y^2 \omega} \right), \frac{4 \sigma_{\omega 2} k}{CD_{K\omega} y^2} \right] \right\}^4 \right\} \quad (6)$$

Known that:

$$CD_{K\omega} = \max \left(2 \rho \sigma_{\omega 2} \frac{1}{\omega} \frac{\partial k}{\partial x_i} \frac{\partial \omega}{\partial x_i}, 10^{-10} \right) \quad (7)$$

Model constants are outlined below:

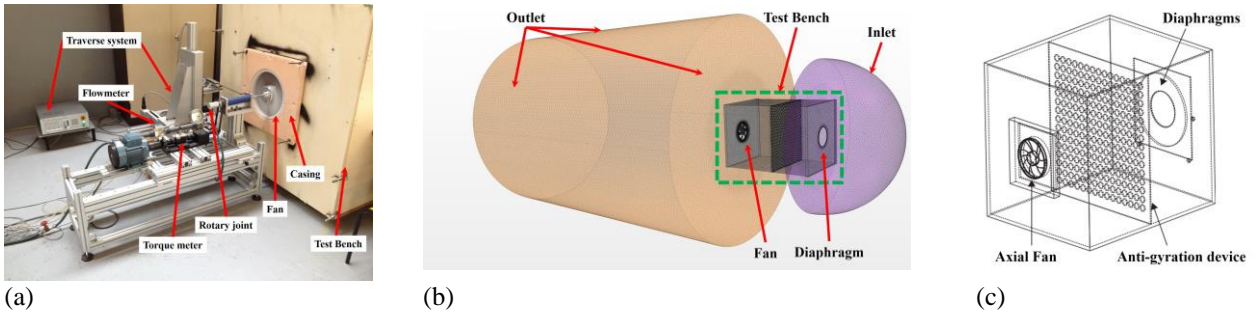


Fig. 3 (a) Experimental assembly (Azzam et al., 2017) (b) Whole numerical 3D-domain (c) Test bench ISO 5801 details.

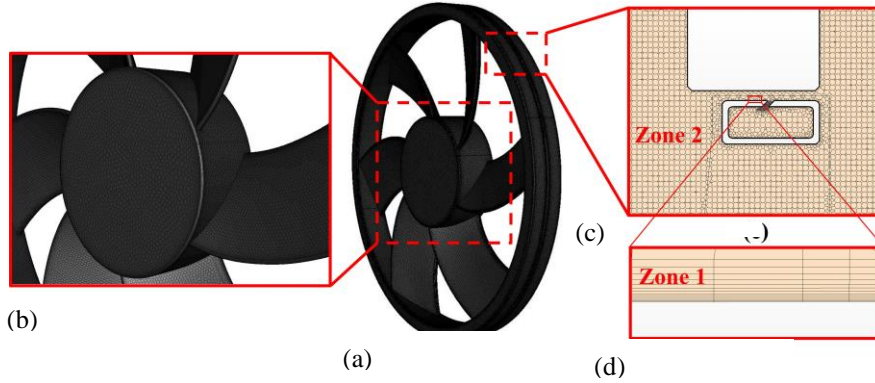


Fig. 4 Mesh topology generated on the fan geometry. (a): Mesh on the fan's walls. (b): Mesh on fan's blades and hub. (c): Mesh near the fan (zone 2). (d): Boundary layer zone (Zone 1).

$$\alpha_1 = \frac{5}{9}, \alpha_2 = 0.44$$

$$\beta_1 = \frac{3}{40}, \beta_2 = 0.0828$$

$$\beta^* = \frac{9}{100}$$

$$\sigma_{k1} = 0.85, \sigma_{k2} = 1$$

$$\sigma_{\omega 1} = 0.5, \sigma_{\omega 2} = 0.856$$

$$P_k = \left(\tau_{ij} \frac{\partial u_i}{\partial x_j}, 10\beta^* k\omega \right)$$

For controlled cases, blowing was specified at the hollow blade inlet at the hub as a mass flow condition as shown in (Fig. 5). We conducted numerical tests with two different injection rates (ξ), denoted as $\xi = 0.4$ and $\xi = 0.8$.

$$\xi = \frac{q_{inj}}{q_{max}} \quad (8)$$

The value of ξ is determined using Eq. (8), which represents the ratio of the injected flow rate (q_{inj}) to the maximum flow rate (q_{max}), available from the air compressor (with a capacity of 1000 liters/min) utilized in our experimental setup (Fig. 3 a).

3. RESULTS AND DISCUSSION

3.1 Impact of Rotating Domain Size on Fan Simulation Accuracy: Investigation and Validation of Numerical Model

The accuracy of simulation results is dependent on several factors, including the rotating domain size. Many studies have demonstrated the significant impact of

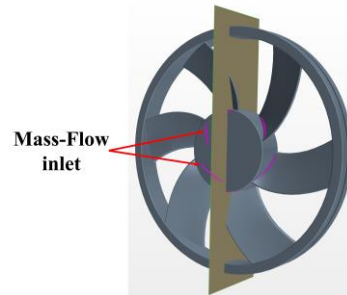


Fig. 5 Cutting plane position for stream trace and the injection inlets positions

rotating domain size on simulation results, including (Zadravec et al., 2007; Gullberg et al., 2011; Kobayashi et al., 2011; Chen et al., 2018; Franzke et al., 2019) especially when the fan operates in low pressure regime. This study investigates the influence of rotating domain size on the numerical accuracy and solver stability by testing several domain dimensions. The axial distance between the fan and the MRF interfaces denoted by λ is varied, while keeping the rotating domain in the radial direction α fixed at the mid-tip clearance for all tested rotational regions (Fig. 6). (Table 1) summarizes the rotating domain dimensions considered in this current analysis.

To account for the unique nature of the main flow downstream of the fan, likely influenced by the presence of the swirling motion zone near the shroud ring and blade sweeping effects. Separate rotating domain dimensions are employed for each diaphragm diameter. In the baseline cases, numerical simulations show that the downstream

Table 1 Rotating domain sizes

Diaphragm Diameter	Rotating Domain	$\frac{\lambda}{D} * 100$ (%)
238	8	2.052
267	7	1.795
300	6	1.54
336	5	1.282
375	4	1.026

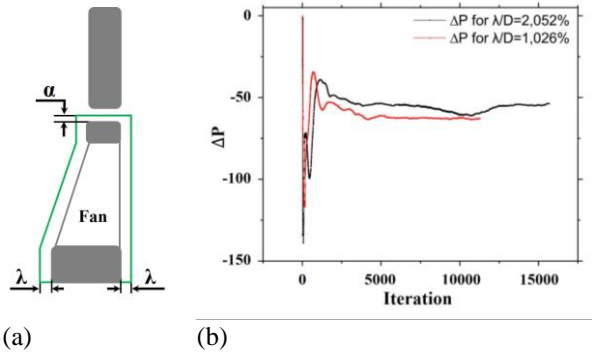


Fig. 6 (a) Rotating domain dimension, (b) Convergence history

flow has an axial main flow at the fan exit for high flow coefficients and a radial flow nature for low flow coefficients confirmed experimentally by (Hurault et al., 2010; Sarraf et al., 2011) and (Kergourlay et al., 2006). Consequently, as the flow rate becomes higher, the rotating domain dimension becomes smaller. The rotating domain dimensions tested in this investigation are sufficient to accurately predict the appropriate orientation of streamlines downstream of the fan and the swirling motion zone size.

To validate the robustness of the adopted numerical model and the appropriate selection of the rotating domain for each diaphragm diameter, the CFD results are compared with previously obtained experimental outcomes from three different hollow blades fans tested on the ISO5801 test bench, referred to as Fan#1 and Fan#2. The first fan, Fan#1, was tested and reported by (Azzam et al., 2017). The comparison of numerical and

experimental results reveals that the characteristic curves obtained numerically using the CFD approach are in good agreement with the experimental ones when the rotating domain is set to an appropriate value for each diaphragm diameter. The effectiveness of the chosen parameters in predicting the fan behaviour for the controlled cases is verified by numerical simulations for two injection rates of $\xi = 0.4$ and $\xi = 0.8$ and both rotation speeds of 1000 and 2000 rpm, using the 16-hole air injection strategy adopted by (Azzam et al., 2017). The numerical simulations follow the same trend as the fan's characteristic curves obtained from experimental tests and show the same gain in aerualic power for the retained configuration of the rotating domain. For these cases, the maximum gain recorded at a rotational speed of 1000 and an injection rate of $\xi = 0.8$. In contrast, data reveals a clear shift when the rotating domain dimension λ was fixed for all diaphragm diameters, especially in controlled cases using 16-Holes strategy, compared to the experimental results.

Moreover, the stability of the solver is a determining factor for the selection of the rotating domain dimension (Fig. 6), where the results are more stable for the optimized considered dimension λ for each studied cases with different diaphragm diameters. As can be seen in (Fig. 6), it clearly shows a fluctuating behaviour even after a considerable number of iterations.

In conclusion, an appropriate size for the rotating domain, based on the diaphragm diameter and flow rate, while utilizing the moving reference frame approach in the CFD numerical model, can accurately replicate the fan behaviour. This ensures the robustness of the numerical model in capturing unsteady phenomena related to the fan's operation. After validating the numerical model adopted in this study, a new control strategy will be proposed in the following sections.

3.2 Control Strategy

In the context of active control using the commonly employed technique of blowing air in specific region of interest, slits with appropriate size and orientation have shown promising results and are frequently used in such circumstances. In current study, slits were proposed as the blowing geometry with various positions tested at the rotating shroud ring.

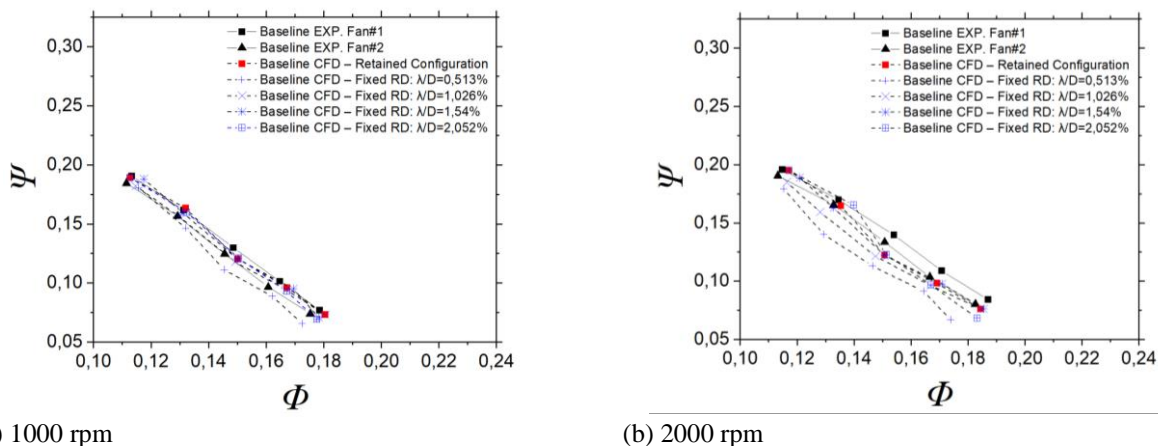
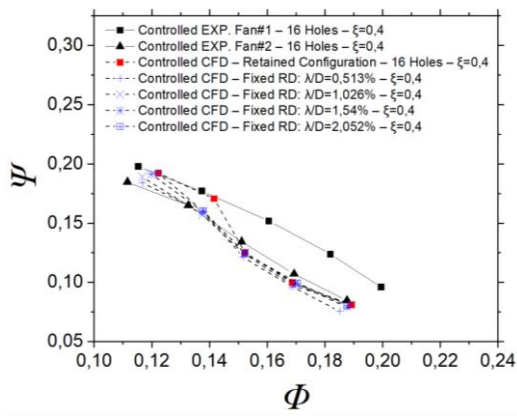
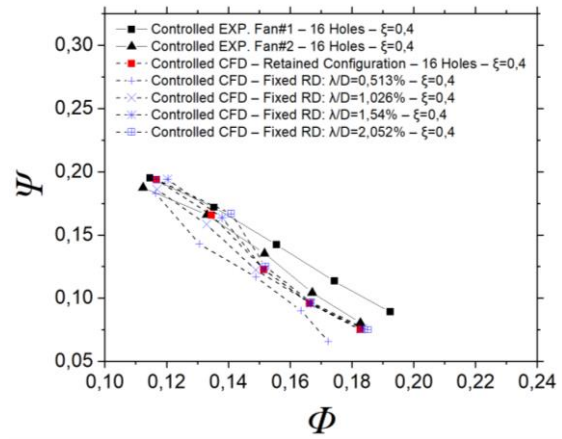


Fig. 7 Fan characteristics at baseline cases

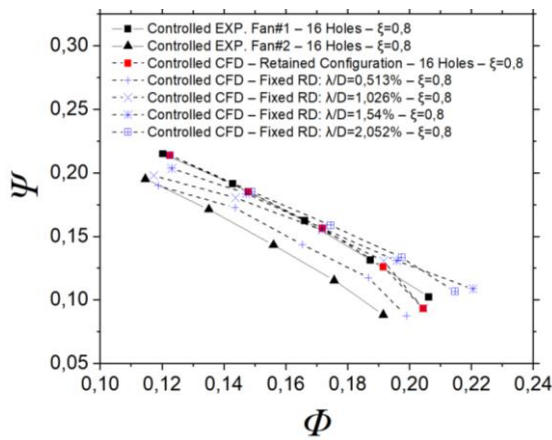


(a) 1000 rpm

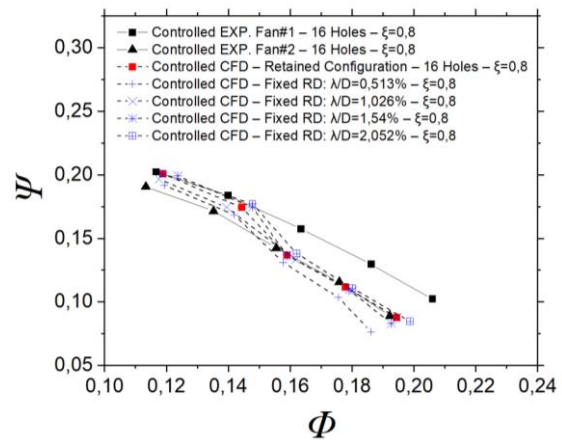


(b) 2000 rpm

Fig. 8 Fan characteristics at controlled cases (16 holes air injection) $\xi = 0.4$

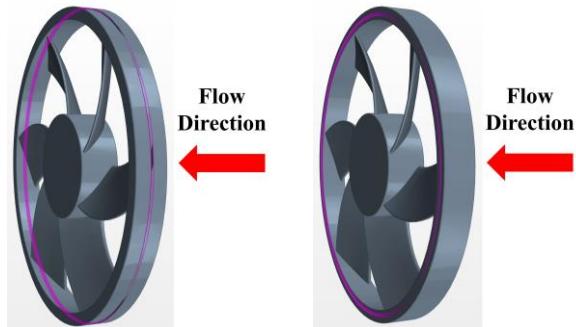


(a) 1000 rpm



(b) 2000 rpm

Fig. 9 Fan characteristics at controlled cases (16 holes air injection) $\xi = 0.8$



(a) Radial injection

(b) Axial injection

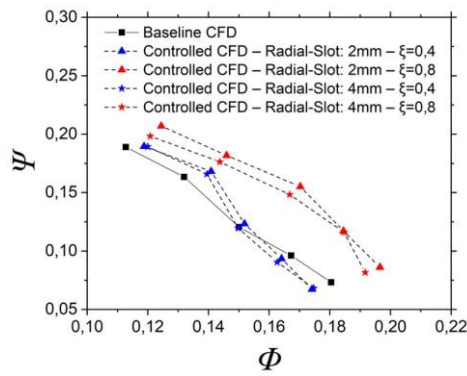
Fig. 10 Geometry, position and orientation of slots

The first proposed strategy, shown in (Fig. 10 a), suggested positioning the slot at the centre of the tip gap over the fan's circumference, with a 45-degree downstream orientation to block the tip leakage flow by building a barrier against it. The second strategy, depicted in (Fig. 10 b), proposed positioning the slot at the side edge of the rim over the fan's periphery, with an orientation of 45 degrees downstream the fan, to eliminate the recirculation zone responsible for creating the leakage flow around the shroud ring, tip clearance gap, and casing walls. The slot dimension was chosen to be about $d = 0.5 T_1$ and $d = T_1$ mm. In the following section, rotational speeds of 1000 and 2000 rpm were investigated, and

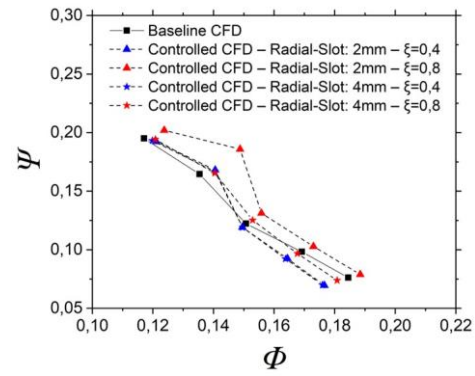
injection rates of $\xi = 0.4$ and $\xi = 0.8$ were examined. The fan's behaviour and aerodynamic performances were carefully studied to assess the effectiveness of the adopted control strategy.

3.3 Control by Radial Injection

To investigate the impact of a chosen control strategy on the leakage flow and its relationship with the aerodynamic performance of an axial fan, a circumferential slot was implemented with dimensions of $d = 2$ mm and $d = 4$ mm, perforated at the mid-tip gap of the fan shroud ring and oriented at a 45-degree angle in the downstream direction towards the tip clearance, as shown in (Fig. 10 a). The baseline characteristics and the new characteristics of the fan corresponding to the controlled cases are presented in (Fig. 11), demonstrating a notable improvement in the fan aerodynamic performance. The maximum enhancement was observed at an injection rate of $\xi = 0.8$, a rotational speed of 1000 rpm, and the $d = 2$ mm slot, likely due to the significant blockage of the leakage flow by the control flow jet, as shown in (Fig. 14). The blockage resulted from the reduced passage section of the control flow through the slot, which increased the jet velocity at the exit and efficiently controlled the leakage flow. However, at higher rotational speeds, the improvement began to decline, likely due to the combined effect of jet velocity speed and the significant centrifugal

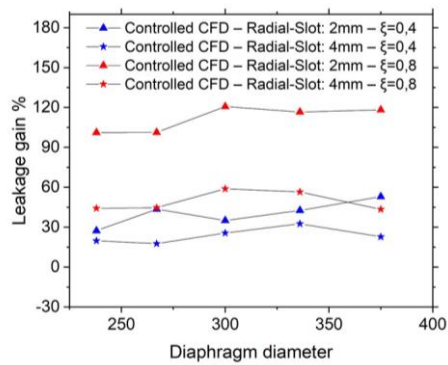


(a) 1000 rpm

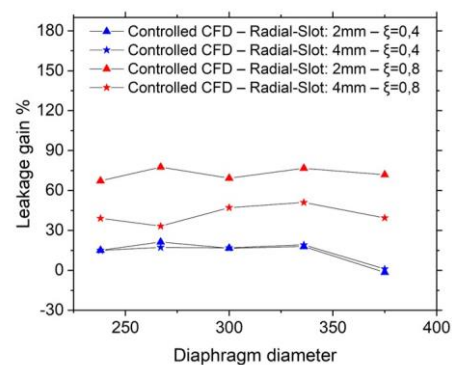


(b) 2000 rpm

Fig. 11 Fan characteristics for controlled cases using radial injection strategy

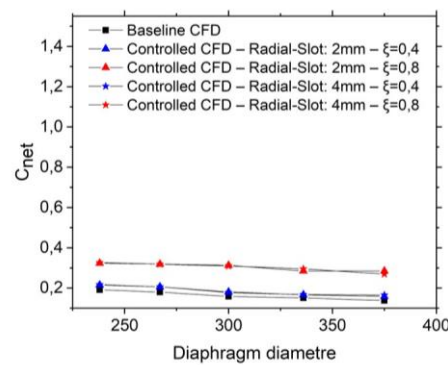


(a) 1000 rpm

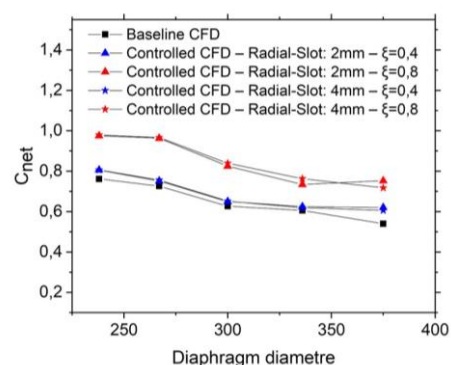


(b) 2000 rpm

Fig. 12 Evolution of the leakage flow gain for the radial injection strategy



(a) 1000 rpm



(b) 2000 rpm

Fig. 13 Evolution of the Net torque for the radial injection strategy

effect resulting in a modification of the swirling zone and a reduction of the main flow's passage section. At a low injection rate of $\xi = 0.4$, the improvement was insignificant, and the flow control was unable to change the flow topology over the fan.

A qualitative analysis of the flow structure, particularly in the region near the fan and the shroud ring, is necessary to understand the contribution of this type of control, its ability to modify flow topology, and its capacity to reduce the previously discussed leakage flow, as demonstrated in (Fig. 12). The flow structure when the maximum improvement of aerodynamic performance and leakage flow reduction was achieved ($\xi = 0.8$, 1000 rpm, and 2 mm slot size) is presented in (Fig. 14). The adopted strategy produced a recirculation zone near the control jet, which entrained fluid from the area upstream of the fan

towards the jet zone and fed the control air flow coming from the downstream slot control air flow. The recirculation zone also changed the direction of the leakage flow to match the main flow. In addition, the control flow changed the fan's operating mode from an axial flow downstream of the fan, as seen in the baseline mode (Figs. 14 a, b, and c), to a radial flow (Figs. 14 d, e, and f). This is similar to the mode of operation at low flow rates, resulting in two recirculation zones in the downstream direction that entrained ambient air towards the fan and discharged it in the radial direction. It can be seen also two small recirculation zones in the walls of the test bench and the disappearance of recirculation bubbles downstream of the fan observed in the baseline case. These recirculation bubbles were likely resulting under the effects of axial flow, hub and recirculation zone close to the shroud ring.

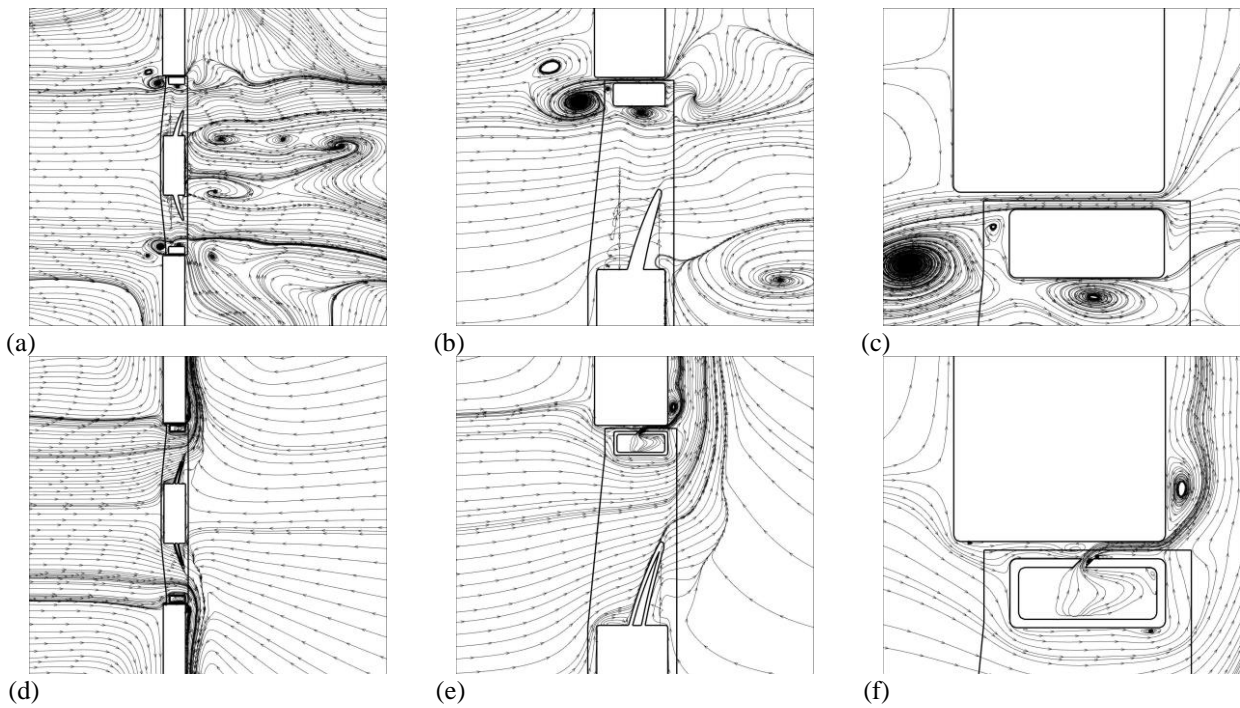
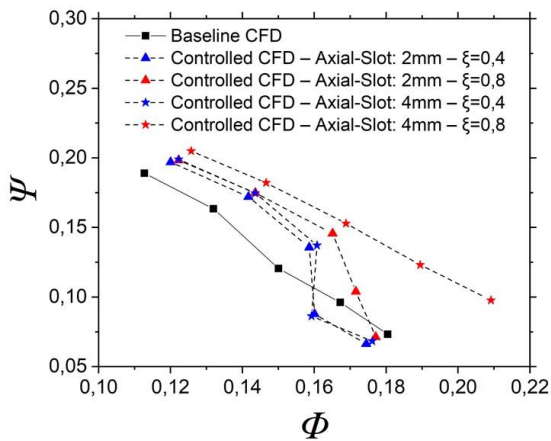
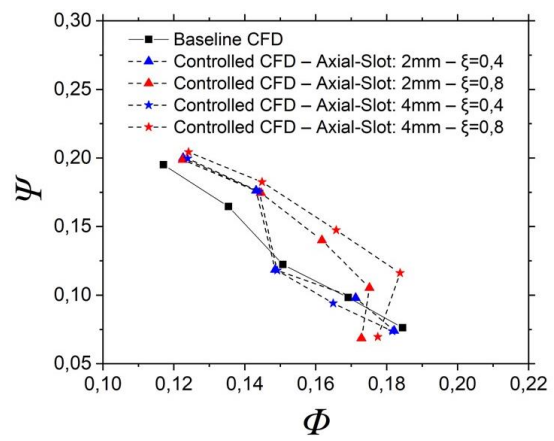


Fig. 14 Flow structure for radial injection at diaphragm diameter 300, rotating speed 1000 rpm and $\xi = 0.8$.
 (a), (b), (c): Baseline case. (d), (e), (f): controlled case

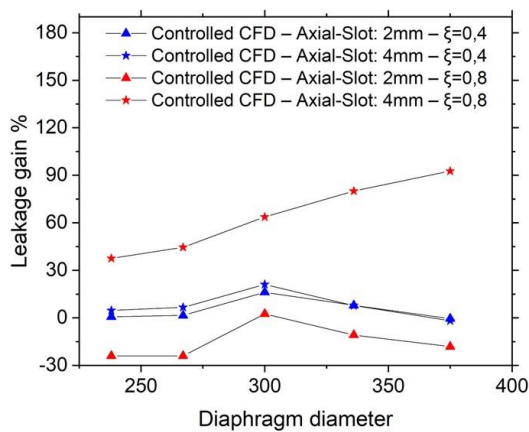


(a) 1000 rpm

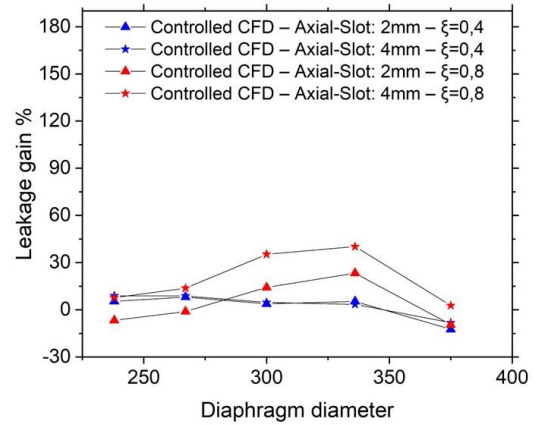


(b) 2000 rpm

Fig. 15 Fan characteristics for controlled cases using axial injection strategy

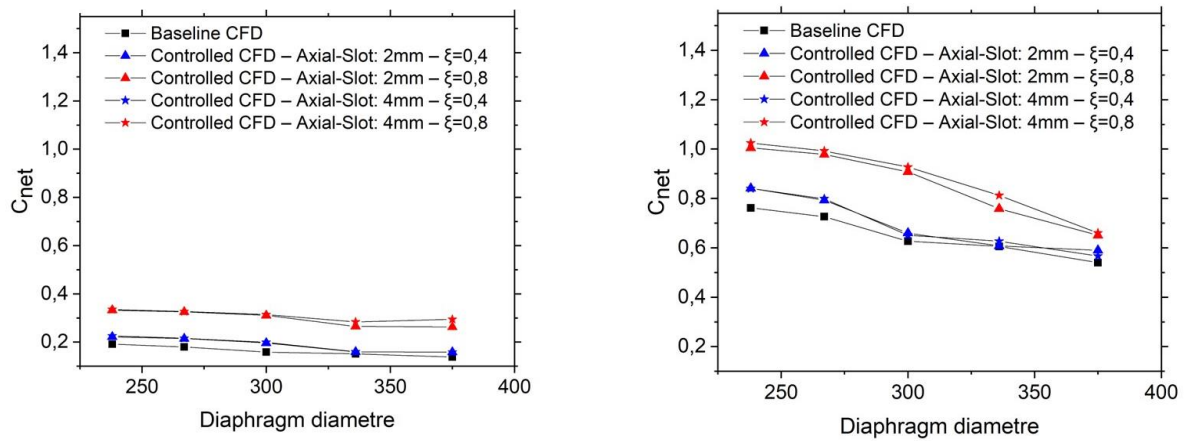


(a) 1000 rpm



(b) 2000 rpm

Fig. 16 Evolution of the leakage flow gain for axial injection strategy



(a) 1000 rpm

(b) 2000 rpm

Fig. 17 Evolution of the net torque for axial injection strategy

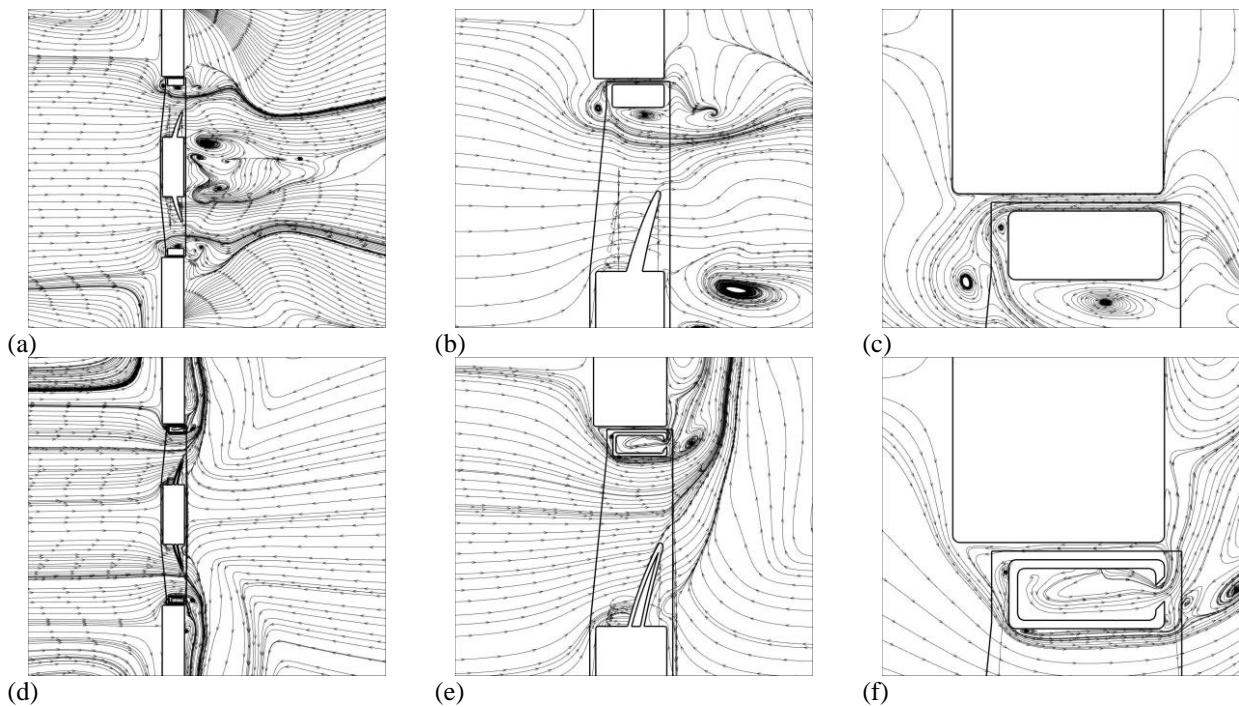


Fig. 18 Flow structure for axial injection at diaphragm diameter 375, rotating speed 1000 rpm and $\xi = 0.8$. (a), (b), (c): Baseline case. (d), (e), (f): controlled case

3.4 Control by Axial Injection

This section discusses the impact of blowing air through side slots of 2 mm and 4 mm wide, perforated in the lateral side of the fan shroud ring on the outer side of the test bench. The objective of this control strategy is to reduce the swirling motion zone around the shroud ring, which was previously stated by (Pereira et al., 2021) caused by periodic phenomena related to the interaction between the main flow and the leakage flow in the vicinity of the shroud ring as discussed by (Canepa et al., 2019). The results show an improvement using this control strategy at high rotation speed and low flow coefficient that is superior to the control when using the circumferential slot.

The improvement in low flow coefficient remains relatively constant as rotational speed and injection rate decrease. The presence of the casing walls in addition to

the centrifugal effect that extends the recirculation zone to the radial direction cause the orientation of the low main flow to the radial direction in these cases, as shown by the characteristic curves, which illustrate a small difference between the rotational speed. The maximum enhancement is achieved with an injection rate of $\xi = 0.8$ and the widest slot of 4 mm. A considerable increase in aerodynamic power (approximately about 56%) was recorded at the rotation speed of 1000 rpm, the injection rate of $\xi = 0.8$, and the diaphragm diameter of 375 mm. The study also observes that at the rotational speed of 2000 rpm in the same flow coefficient for the two injection rates, the lateral injection has negative effect on both the aerodynamic power and the aerodynamic performances. This caused an increase in the leakage flow, and these two scenarios will be the subject of a qualitative analysis in order to fully understand the influence of the control on the flow topology shown in (Fig. 18) and (Fig. 19).

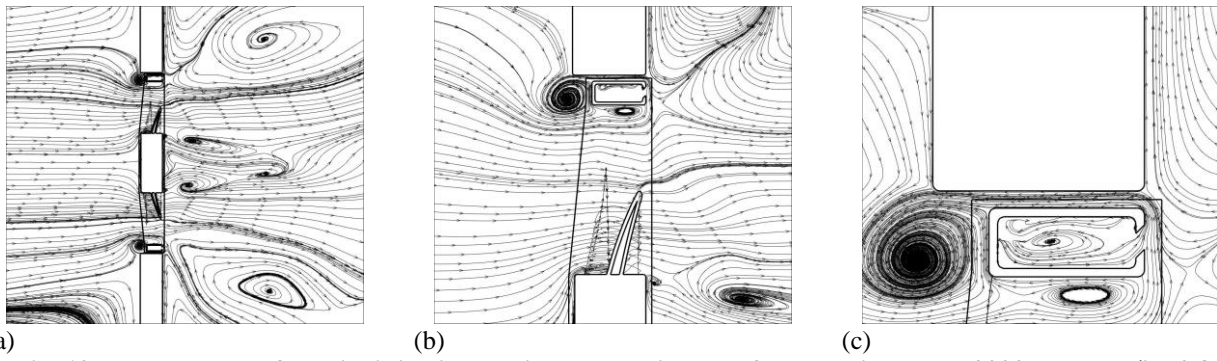


Fig. 19 Flow structure for axial injection at diaphragm diameter 375, rotating speed 2000 rpm and $\xi = 0.8$

In the first case where the improvement was maximum corresponding to maximum reduction in the leakage flow, the adopted control strategy also contributes to the change of the fan's operating mode from the axial to the radial one. However, in this case, the radial air discharge is wider in the axial direction compared to the case of the diaphragm diameter of 300 mm described in the previous part. This is probably due to the high main flow rate. In this case, it is observed also a development of two counter-rotating vortices close to the control jet flow on the internal side, which probably influence the direction of the main flow. Furthermore, a small recirculation zone upstream of the fan close to the rim can be seen, which sucks an amount of the control jet to the backward direction in the tip clearance as a leakage flow, which explains its persistence.

Figure 19 displays the simulation results for the 375-diaphragm diameter, the injection rate of $\xi = 0.8$, and the rotational speed of 2000 rpm where the control has a negative impact on the aerodynamic performance. The high rotational speed generates two significant asymmetric counter-rotating recirculation zones with regard to the axis of the fan, which causes the axial main flow to be deviated radially. Additionally, a larger recirculation zone can be seen upstream of the fan and close to the rim than in the rotation speed of 2000 rpm. This increases the leakage flow by sucking much of the air from the area downstream of the fan in addition to the control flow through the leakage gap. The recirculation bubble under the rim was also growing up.

3.5 Leakage Flow Reduction

To investigate the impact of the adopted control strategy on leakage flow and its correlation to the aerodynamic performance of the tested axial fan. The leakage flow gain is shown in (Figs 12 and 16), computed at the same location (blue section) as that taken into account by (Pereira et al., 2021) (Fig. 20), which is situated roughly 25% of the tip gap width from the exit surface. It is noticed that the radial injection strategy using circumferential slot, which involves blowing air towards the tip clearance at a high jet speed, obstructs the leakage flow across the entire tip gap circumference, contributing more to the reduction of the leakage flow than the side slot strategy. Additionally, there exists an inverse relationship between the passage section and the reduction in leakage flow. A gain value of over 120% spotted in (Fig. 12 a) was recorded at a rotation speed of 1000 rpm and an injection rate of $\xi = 0.8$ for the 2 mm circumferential slot considered

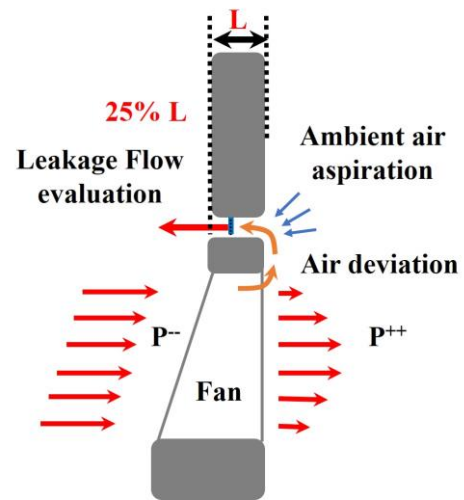


Fig. 20 Leakage flow evaluation position (Pereira et al., 2021)

to be the favourable controlled situation where the jet speed was at its highest value. However, this improvement diminishes as the rotational speed is increased, as seen in (Fig. 12 b), where the maximum leakage flow reduction was approximately 77%, and the leakage flow persists in small amounts.

3.6 Resistive Net Torque

Figures 13 a and b and Figs 17 a and b illustrate the evolution of the resistive net torque generated by the fan walls, obtained through numerical simulations for all implemented control strategies, in comparison with the baseline configuration. At 1000 rpm and low injection rate corresponding to $\xi = 0.4$, a slight increase in the net torque is recorded, likely due to the interaction between the jet flow control and the radial main flow downstream of the fan, which contributes to the creation of recirculation zones, particularly near the shroud ring. For the injection rate of $\xi = 0.8$, this net torque consistently rises compared to the injection rate of $\xi = 0.4$. However, this difference between the two injection rates seems to weaken as the rotational speed increases, especially for the high flow coefficient. This is evident in the case of rotational speed of 2000 rpm (Fig. 13 b) and (Fig. 17 b), where it can be noticed that a significant growth in the net torque for all adopted strategies and flow injection rates with close ranges is clearly identified. The highest increase in net torque is always recorded in the side slot strategy.

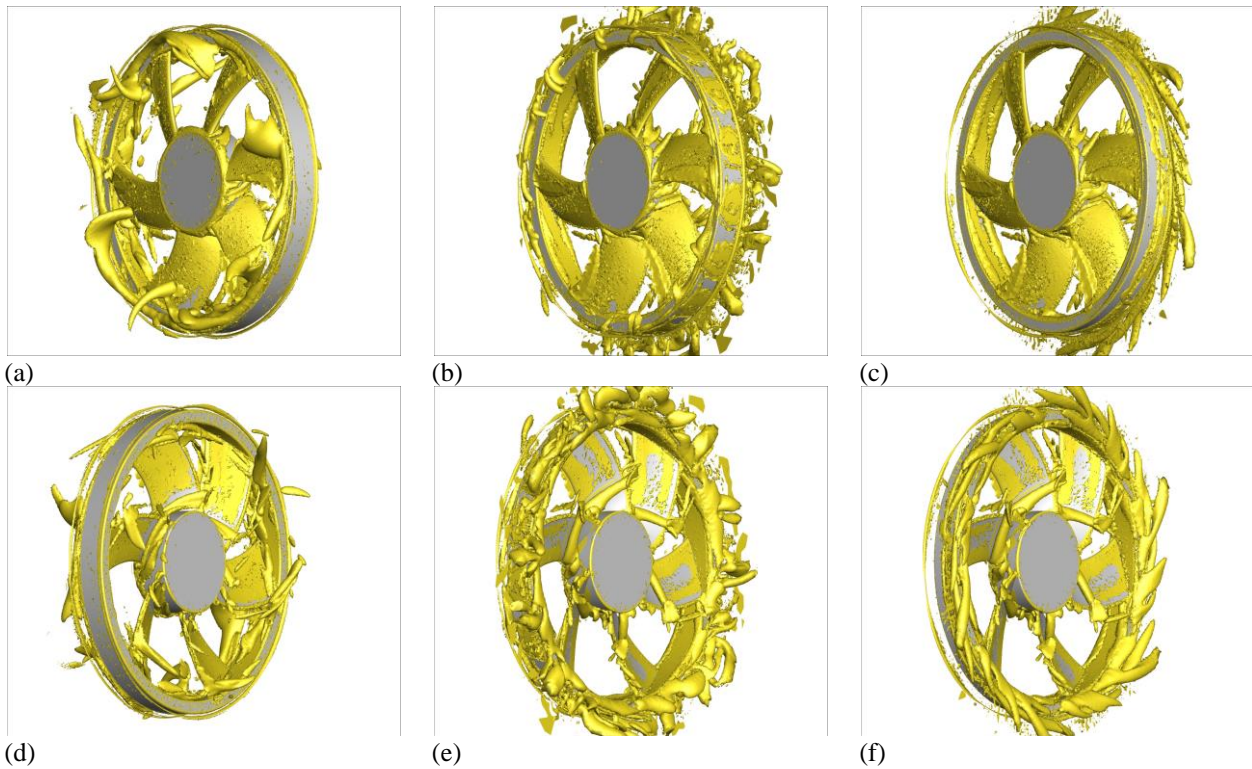


Fig. 21 Vorticity analyses using Q criterion for diaphragm diameter 300 mm, rotating speed 1000 rpm and $\xi = 0.8$. (a), (d): Baseline case. (b), (e): 16 holes controlled case. (c), (f): Controlled case using radial injection by 2 mm circumferential slot. (Flow from left to right)

From the above, it can be concluded that friction is the factor that has a great influence on the increase of net torque. Contrary to the 16-hole control strategy used by (Azzam et al., 2017) which is supported numerically in the first part of this study. A good orientation of these holes generates an important flow rate at their output in forms of high-speed jet oriented in the opposite direction of the rotational flow, contributing to the reduction of the net torque. However, the impact of friction then returns for high rotational speed.

3.7 Vorticity Analyses

The yellow-colored iso-surface of the Q criterion is presented in (Fig. 21), (Fig. 22), and (Fig. 23) for a specific value of 50000 s^{-2} to aid in visualizing the swirling zone caused by the interaction between the leakage and main flow. This vortex pattern confirms the periodic nature of the flow around the fan's shroud ring as described in (Canepa et al., 2019) and affects the fan's downstream airflow. The Q criterion contour and stream traces shown in (Fig. 14), (Fig. 18), and (Fig. 19) at plane 1 shown in figure (Fig. 5) are well aligned. The shrouded fan's tip leakage vortex, which is likely the main source of sound emission, originates as a leakage flow from the clearance gap in the baseline scenario and is subsequently reintroduced into the main flow between two succeeding blades. The swirling zone disappears with the control method used in this study, but downstream of the fan, it creates vortices that modify the flow topology by drawing the main flow in the radial direction due to centrifugal forces. The 16-hole air injection control used by (Azzam et al., 2017) results in the continuation of this swirling

zone but not in a periodic manner. Additionally, it is noticeable that the high rotation speed contributes to the increase of the leakage flow and the swirling zone near the shroud ring, adversely affecting the aerodynamic performances for the case of a 375 mm diaphragm diameter, injection rate of $\xi = 0.8$, and a rotation speed of 2000 rpm.

4. CONCLUSION

This study explores the use of a numerical approach for active flow control on an axial fan. Perforated slots at the shroud ring, midway on the peripheral surface, and midway on the side surface are used as control outputs for flow rate. The influence of these control strategies on aerodynamic performance, flow topology, and the relationship between aerodynamic power gain and leakage reduction is examined.

In the first part, the study highlights the sensitivity of numerical simulations to the rotation domain scaling, where an appropriate size for each considered five fan flow rates is carefully chosen. A search for the rotation domain size that provides the best agreement between numerical results and experimental data is performed for each studied point at every single flow rate. In the second part, the study presents and analyses the results of numerical simulations for controlled cases and a concise comparison with fan's baseline data is made, throughout exploring fan characteristics, net torque, and leakage flow rate. The investigation covers two rotation speeds and two injection rates.

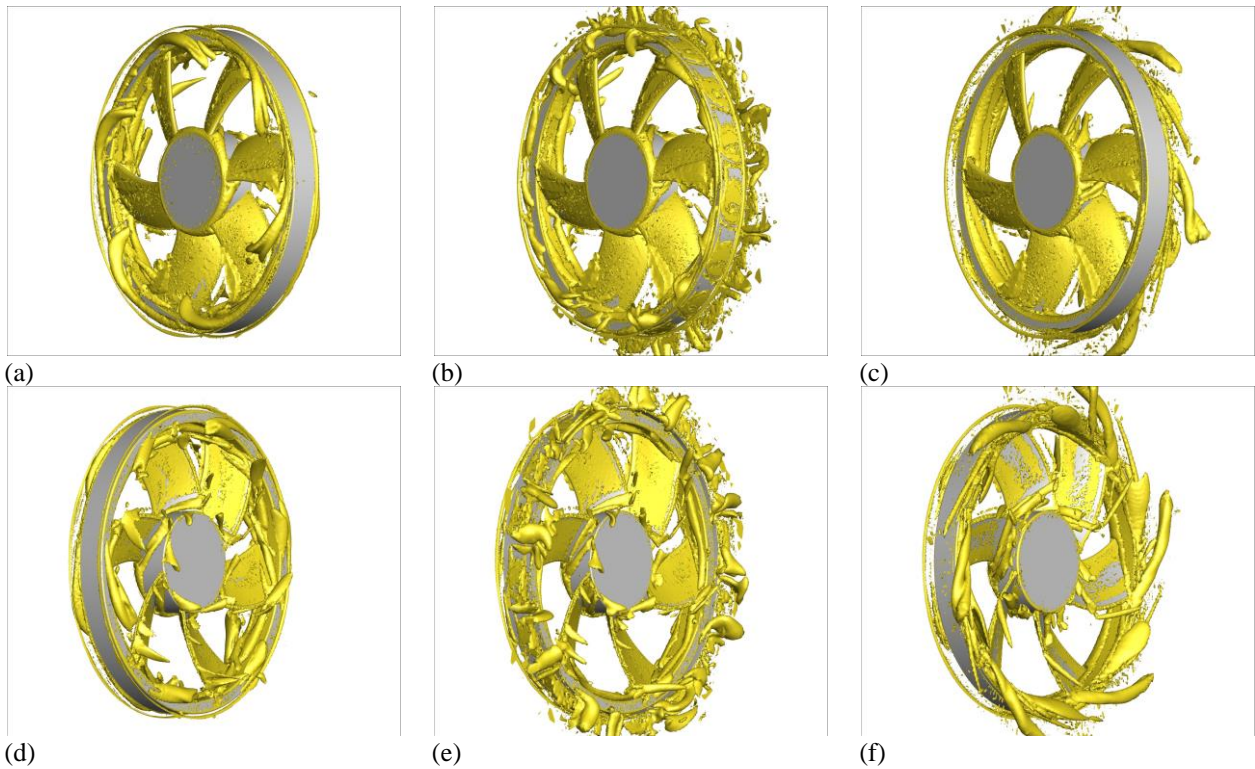


Fig. 22 Vorticity analyses using Q criterion for diaphragm diameter 375 mm, rotating speed 1000 rpm and $\xi = 0.8$. (a), (d): Baseline case. (b), (e): 16 holes controlled case. (c), (f): Controlled case using axial injection by 4 mm side slot. (Flow from left to right)

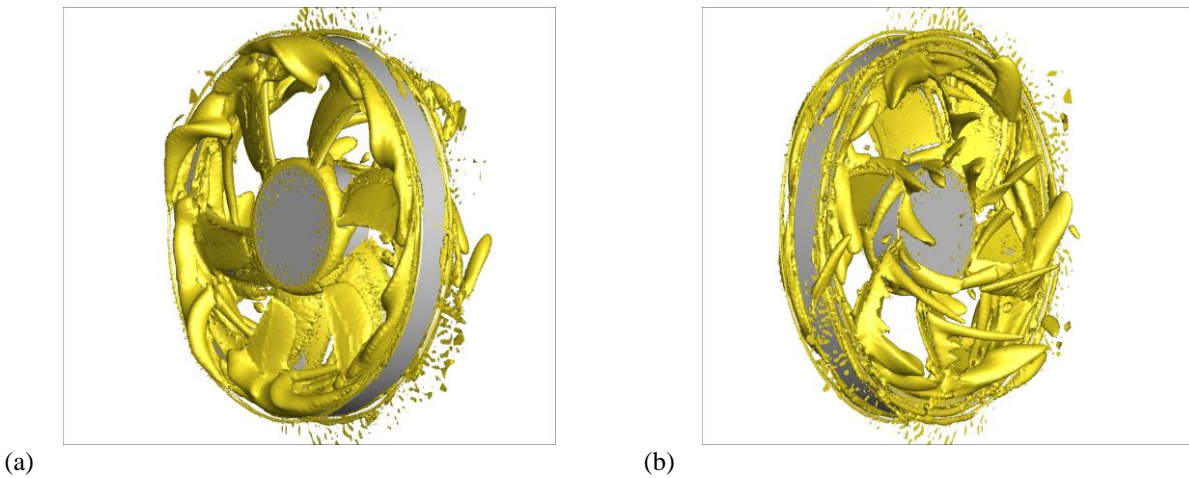


Fig. 23 Vorticity analyses using Q criterion for the diaphragm diameter 375 mm, rotating speed 2000 rpm and $\xi = 0.8$, Controlled case using axial injection by 4 mm side slot. (Flow from left to right)

Overall, the numerical simulations with the control strategy show promising results, indicating potential improvements in the overall aerodynamic performances and flow topology. The maximum improvement observed was approximately 56%, achieved at a rotation speed of 1000 rpm, injection rate corresponding to $\xi = 0.8$ and a diaphragm diameter of, $D = 375$ mm. Furthermore, the CFD analysis of the controlled cases with circumferential slots show a gain of over 120% in the leakage flow, indicating that the flow in the working space was reversed in the same direction as the main flow. In addition, qualitative analysis indicates that the control strategy contributes to the modification of flow topology,

particularly in the swirling zone near the shroud ring, which significantly affects the generation of leakage flow and the orientation of the main flow. Moreover, future works, supported by an in-depth discussion, will be devoted to flow topology and the processes influencing its evolution, as well as the impact of flow control to its evolution.

Moreover, an increase in the fan's net torque is observed in all studied cases when the new control strategies were applied. This is likely due to flow friction generated either on the casing or on the inner walls side of the fan facing the blade outlet, thus creating a favourable

pressure zone. Therefore, the net torque increases as both fan's rotation speed and injection rate were increased.

In summary, the research principles and methods we have developed in our paper are adaptable and applicable to a wide range of industries and research domains, such as aerospace engineering, heating, ventilation, and air conditioning (HVAC) control, industrial processes, renewable energy, and many others. These applications have the potential to enhance efficiency, reduce energy consumption, and address environmental challenges in various sectors.

CONFLICT OF INTEREST

The author declares that there is no conflict of financial or non-financial interest to disclose.

AUTHORS CONTRIBUTION

A. Bouanik: Data curation, Investigation, Software, Visualization, Formal analysis, Writing – original draft; **T. Azzam:** Data curation, Resources, Methodology, Software; **N. Abbasnezhad:** Visualization, Writing – review & editing; **A. Larabi:** Data curation, Methodology, Visualization, Writing – review & editing; **M. Mekadem:** Methodology, Supervision; **F. Bakir:** Methodology, Supervision, Writing – review & editing.

REFERENCES

- Azzam, T., Paridaens, R., Ravelet, F., Khelladi, S., Oualli, H., & Bakir, F. (2017). Experimental investigation of an actively controlled automotive cooling fan using steady air injection in the leakage gap. *Proceedings of the Institution of Mechanical Engineers, Part A: Journal of Power and Energy*, 231(1), 59–67. <https://doi.org/10.1177/0957650916688120>
- Boudet, J., Cahuzac, A., Kausche, P., & Jacob, M. C. (2015). Zonal large-eddy simulation of a fan tip-clearance flow, with evidence of vortex wandering. *Journal of Turbomachinery*, 137(6), 1–9. <https://doi.org/10.1115/1.4028668>
- Buisson, M., Ferrand, P., Soulat, L., Aubert, S., Moreau, S., Rambeau, C., & Henner, M. (2013). Optimal design of an automotive fan using the Turb'Opty meta-model. *Computers and Fluids*, 80(1), 207–213. <https://doi.org/10.1016/j.compfluid.2012.03.015>
- Morris, S. C. & Foss, J. F. (2001). An Aerodynamic Shroud for Automotive Cooling Fans. *Journal of Fluids Engineering*, 123(2), 287–292. <https://doi.org/10.1115/1.1359212>
- Canepa, E., Cattanei, A., Mazzocut Zecchin, F., Milanese, G., & Parodi, D. (2016). An experimental investigation on the tip leakage noise in axial-flow fans with rotating shroud. *Journal of Sound and Vibration*, 375, 115–131. <https://doi.org/10.1016/j.jsv.2016.04.009>
- Canepa, E., Cattanei, A., Mazzocut Zecchin, F., & Parodi, D. (2019). Large-scale unsteady flow structures in the leakage flow of a low-speed axial fan with rotating shroud. *Experimental Thermal and Fluid Science*, 102, 1–19. <https://doi.org/10.1016/j.expthermflusci.2018.10.020>
- Chen, S., Gong, Y., & Zeng, C. (2022). Experimental investigation of hole-type bleed for active flow control in an axial compressor cascade with tip clearance. *Aerospace Science and Technology*, 128, 107790. <https://doi.org/10.1016/j.ast.2022.107790>
- Chen, S., Zhou, Z., Meng, Q., Wang, S., & Zhou, X. (2017). Experiment study of the winglet-cavity tip on the aerodynamic performance in a turbine cascade. *Proceedings of the Institution of Mechanical Engineers, Part A: Journal of Power and Energy*, 231(7), 676–685. <https://doi.org/10.1177/0957650917720560>
- Chen, W., Liu, S., Gao, Y., Zhang, H., Arens, E., Zhao, L., & Liu, J. (2018). Experimental and numerical investigations of indoor air movement distribution with an office ceiling fan. *Building and Environment*, 130, 14–26. <https://doi.org/10.1016/j.buildenv.2017.12.016>
- Eberlinc, M., Širok, B., Dular, M., & Hočevcar, M. (2009). Modification of axial fan flow by trailing edge self-induced blowing. *Journal of Fluids Engineering, Transactions of the ASME*, 131(11), 1111041–1111047. <https://doi.org/10.1115/1.4000345>
- Fischer, A., König, J., Czarske, J., Rakenius, C., Schmid, G., & Schiffer, H. P. (2013). Investigation of the tip leakage flow at turbine rotor blades with squealer cavity. *Experiments in Fluids*, 54(2). <https://doi.org/10.1007/s00348-013-1462-1>
- Franzke, R., Sebben, S., Bark, T., Willeson, E., & Broniewicz, A. (2019). Evaluation of the multiple reference frame approach for the modelling of an axial cooling fan. *Energies*, 1–14. <https://doi.org/10.3390/en12152934>
- Gullberg, P., Lofdahl, L., & Nilsson, P. (2011). Cooling airflow system modeling in CFD using assumption of stationary flow. *SAE Technical Papers*, 1. <https://doi.org/10.4271/2011-01-2182>
- Haghighatjoo, H., Yadegari, M., & Bak Khoshnevis, A. (2022). Optimization of single-obstacle location and distance between square obstacles in a curved channel. *The European Physical Journal Plus*, 137(9), 1042. <https://doi.org/10.1140/epjp/s13360-022-03260-y>
- Heinrich, M., Khaleghi, H., & Friebe, C. (2020). Effect of circumferential casing treatment on low-speed contra-rotating fans. *Journal of Applied Fluid Mechanics*, 13(6), 1719–1726. <https://doi.org/10.47176/jafm.13.06.31492>
- Hur, K. H., Haider, B. A., & Sohn, C. H. (2021). A numerical study on the performance of a magnesium-based automotive cooling fan with bead structure. *Journal of Applied Fluid Mechanics*, 14(1), 11–21. <https://doi.org/10.47176/jafm.14.01.31222>

- Hurault, J., Kouidri, S., Bakir, F., & Rey, R. (2010). Experimental and numerical study of the sweep effect on three-dimensional flow downstream of axial flow fans. *Flow Measurement and Instrumentation*, 21(2), 155–165. <https://doi.org/10.1016/j.flowmeasinst.2010.02.003>
- International Organization for Standardization (2007). Ventilateurs industriels - Essais aérauliques sur circuits normalisés (ISO 5801).
- Kameier, F., & Neise, W. (1997). Rotating blade flow instability as a source of noise in axial turbomachines. *Journal of Sound and Vibration*, 203(5), 833–853. <https://doi.org/10.1006/jsvi.1997.0902>
- Kergourlay, G., Kouidri, S., Rankin, G. W., & Rey, R. (2006). Experimental investigation of the 3D unsteady flow field downstream of axial fans. *Flow Measurement and Instrumentation*, 17(5), 303–314. <https://doi.org/10.1016/j.flowmeasinst.2006.05.002>
- Kobayashi, Y., Kohri, I., & Matsushima, Y. (2011). Study of influence of MRF method on the prediction of the engine cooling fan performance. SAE 2011 World Congress and Exhibition. <https://doi.org/10.4271/2011-01-0648>
- Larabi, A., Pereira, M., Ravelet, F., Azzam, T., Oualli, H., Menfoukh, L., & Bakir, F. (2022). Numerical investigation of parietal pressure distribution on NACA0012 wing controlled by micro-cylindrical rod arranged in tandem. *Progress in Computational Fluid Dynamics, An International Journal*, 1(1), 1. <https://doi.org/10.1504/pcfd.2022.10051919>
- Lucas, A., Danlos, A., Shirinbayan, M., Motaharnejad, V., Paridaens, R., Benfriha, K., Bakir, F., & Tcharkhtchi, A. (2019). Conventional rotational molding process and aerodynamic characteristics of an axial-flow hollow blades rotor. *International Journal of Advanced Manufacturing Technology*, 104(1–4), 1183–1194. <https://doi.org/10.1007/s00170-019-03962-1>
- Luo, D., Huang, D., Sun, X., Chen, X., & Zheng, Z. (2017). A computational study on the performance improvement of low-speed axial flow fans with microplates. *Journal of Applied Fluid Mechanics*, 10(6), 1537–1546. <https://doi.org/10.29252/jafm.73.245.27492>
- Nadeau, S. (2005). Integral tip seal in a fan-shroud structure Siemens VDO Automotive Inc. US Patent 56874990.
- Neuhaus, L., & Neise, W. (2007). Active control to improve the aerodynamic performance and reduce the tip clearance noise of axial turbomachines with steady air injection into the tip clearance gap. Active flow control (Notes on Numerical Fluid Mechanics and Multidisciplinary Design), Berlin/Heidelberg: Springer. [https://doi.org/10.12968/s1478-2774\(22\)50458-5](https://doi.org/10.12968/s1478-2774(22)50458-5)
- Park, K., Choi, H., Choi, S., & Sa, Y. (2019). Effect of a casing fence on the tip-leakage flow of an axial flow fan. *International Journal of Heat and Fluid Flow*, 77, 157–170. <https://doi.org/10.1016/j.ijheatfluidflow.2019.04.005>
- Pereira, M., Ravelet, F., Azzouz, K., Azzam, T., Oualli, H., Kouidri, S., & Bakir, F. (2021). Improved aerodynamics of a hollow-blade axial flow fan by controlling the leakage flow rate by air injection at the rotating shroud. *Entropy*, 23(7). <https://doi.org/10.3390/e23070877>
- Pogorelov, A., Meinke, M., & Schröder, W. (2016). Effects of tip-gap width on the flow field in an axial fan. *International Journal of Heat and Fluid Flow*, 61, 466–481. <https://doi.org/10.1016/j.ijheatfluidflow.2016.06.009>
- Sarraf, C., Nouri, H., Ravelet, F., & Bakir, F. (2011). Experimental study of blade thickness effects on the overall and local performances of a controlled vortex designed axial-flow fan. *Experimental Thermal and Fluid Science*, 35(4), 684–693. <https://doi.org/10.1016/j.expthermflusci.2011.01.002>
- Sheng, C., & Zhao, Q. (2017). Numerical investigations of fan-in-wing aerodynamic performance with active flow control. *Journal of Aircraft*, 54(6), 2317–2329. <https://doi.org/10.2514/1.C034134>
- Tiainen, J., Grönman, A., Jaatinen-Värri, A., & Backman, J. (2018). Flow control methods and their applicability in low-reynolds-number centrifugal compressors - A review. *International Journal of Turbomachinery, Propulsion and Power*, 3,(1). <https://doi.org/10.3390/ijtpp3010002>
- Wallis, A. M., Denton, J. D., & Demargne, A. A. J. (2001). The control of shroud leakage flows to reduce aerodynamic losses in a low aspect ratio, shrouded axial flow turbine. *Journal of Turbomachinery*, 123(2), 334–341. <https://doi.org/10.1115/1.1354143>
- Yadegari, M. (2021). An optimal design for S-shaped air intake diffusers using simultaneous entropy generation analysis and multi-objective genetic algorithm. *The European Physical Journal Plus*, 136(10), 1019. <https://doi.org/10.1140/epjp/s13360-021-01999-4>
- Yadegari, M., & Bak Khoshnevis, A. (2020a). Entropy generation analysis of turbulent boundary layer flow in different curved diffusers in air-conditioning systems. *European Physical Journal Plus*, 135(6). <https://doi.org/10.1140/epjp/s13360-020-00545-y>
- Yadegari, M., & Bak Khoshnevis, A. (2020b). Numerical study of the effects of adverse pressure gradient parameter, turning angle and curvature ratio on turbulent flow in 3D turning curved rectangular diffusers using entropy generation analysis. *European Physical Journal Plus*, 135(7), 1–21. <https://doi.org/10.1140/epjp/s13360-020-00561-y>
- Yadegari, M., & Bak Khoshnevis, A. (2021). Investigation of entropy generation, efficiency, static and ideal pressure recovery coefficient in curved annular

diffusers. *The European Physical Journal Plus*, 136(1), 69. <https://doi.org/10.1140/epjp/s13360-021-01071-1>

You, D., Wang, M., Moin, P., & Mittal, R. (2006). Effects of tip-gap size on the tip-leakage flow in a turbomachinery cascade. *Physics of Fluids*, 18(10). <https://doi.org/10.1063/1.2354544>

Zadravec, M., Basic, S., & Hribersek, M. (2007). The influence of rotating domain size in a rotating frame of

reference approach for simulation of rotating impeller in a mixing vessel. *Journal of Engineering Science and Technology*, 2(2), 126–138. <https://jestec.taylors.edu.my/V2Issue2.html>

Zhu, T., & Carolus, T. H. (2013). *Experimental and numerical investigation of the tip clearance noise of an axial fan*. Proceedings of the ASME Turbo Expo, American Society of Mechanical Engineers. <https://doi.org/10.1115/GT2013-94100>